Supporting Information

For

Yellow thermally activated delayed fluorescence emitters based on pyridyl-acridone acceptor for organic light-emitting diodes

Hongyu Chen,[a] Jingjie Yang,[a] Jing Jin,[c] Jiahui Wang,[a] Jiaxin Wang,[a] Jiuyan Li,*[a,b] Yongqiang Mei,*[d] Di Liu*[c]

[a] Frontier Science Center for Smart Materials, College of Chemical Engineering, Dalian University of Technology, 2 Linggong Road, Dalian, 116024, China.

Email: jiuyanli@dlut.edu.cn

[b] Shandong Laboratory of Advanced Materials and Green Manufacturing at Yantai, Yantai Economic and Technological Development Zone, 300 Changjiang Road, Yantai, China.

[c] Frontier Science Center for Smart Materials, College of Chemistry, Dalian University of Technology, 2 Linggong Road, Dalian, 116024, China.

Email: liudi@dlut.edu.cn

[d] College of Environment and Chemical Engineering, Dalian University, Dalian 116622, China.

E-mail: meiyongqiang@dlu.edu.cn

1. Experimental section

1.1 General information

^{1}H NMR and ^{13}C NMR spectra were recorded on a Bruker Avance II 500 spectrometer at 500 MHz in $CDCl_3$. Mass spectra were obtained using matrix-assisted laser desorption/ionization (MALDI) micro mass spectrometry (MS). The ultraviolet-visible (UV-vis) absorption spectra were measured on a PerkinElmer Lambda 650 spectrophotometer. Photoluminescence (PL) spectra in various solvents and transient fluorescence decay curves in doped films were obtained using an Edinburgh Instruments FLS1000 spectrometer. Low-temperature phosphorescence spectra were measured at 77 K with a delay time of 6 ms, and the instrument gate time was set to 6 ms during the measurement. Cyclic voltammetry (CV) measurements were conducted using a CHI610E electrochemical workstation. The three-electrode system consisted of a glassy carbon working electrode, a platinum wire counter electrode, and a saturated calomel electrode (SCE) as the reference. Measurements were carried out at room temperature under a nitrogen atmosphere in deoxygenated DMF containing 0.1 M Bu_4NPF_6 as the supporting electrolyte, at a scan rate of 100 mV s^{-1}. Absolute PLQYs in doped films were determined using a Hamamatsu C11347 spectrometer. Density Functional Theory (DFT) and time-dependent DFT (TD-DFT) calculations were performed using Gaussian 09 software. Natural transition orbitals (NTOs) were analyzed using Multiwfn 3.8 to characterize the electronic transitions involved in the excitation process.

1.2 OLED fabrication and measurements

OLEDs were fabricated via substrate pretreatment and sequential vacuum deposition of the functional layers. Pre-patterned ITO substrates were treated with ultraviolet-ozone for 30 min to increase the ITO work function. The substrates were transferred to a vacuum evaporation chamber, where functional layers were sequentially deposited under high vacuum conditions. After deposition, devices were cooled for 30 min before being removed from the chamber. Device performance was evaluated at room temperature in air. The current density-voltage-brightness (*J-V-B*) curves of the devices were measured using a Konica Minolta CS200 colorimeter and a Keithley 2400 source-measure unit. The electroluminescence (EL) spectra and CIE coordinates were recorded with a Hamamatsu C9920 spectrometer. Forward-viewing EQE was calculated from current efficiency, the EL spectra, and the human eye photopic sensitivity, under the assumption of Lambertian emission.

1.3 Syntheses of compounds

All chemicals for compound syntheses were purchased from commercial sources and used as received unless stated otherwise. The key intermediate 3-fluoro-6-(trifluoromethyl)acridin-9(10*H*)-one (3-F-6-CF_3-AD) was synthesized following a literature procedure.[22]

1.3.1 General procedure for synthesis of 3-F-6-CF_3-AD-Py

To a dry 100 mL three-necked flask were added 3-fluoro-6-(trifluoromethyl)acridin-9(10*H*)-one (2.50 g, 8.89 mmol), 2-bromo-5-methylpyridine

(1.86 g, 11.56 mmol), potassium carbonate (1.84 g, 13.3 mmol), copper(I) iodide (0.17 g, 0.88 mmol), and 2,2,6,6-tetramethyl-3,5-heptanedione (0.31 g, 1.68 mmol). The mixture was dissolved in anhydrous N,N-dimethylformamide (DMF) and heated at reflux (156 °C) under a nitrogen atmosphere for 24 h. After completion of the reaction, the solvent was removed under reduced pressure, and the residue was extracted with dichloromethane (DCM, 3×50 mL). The combined organic layers were dried over anhydrous sodium sulfate and concentrated by rotary evaporation to afford the crude product, which was purified by column chromatography (eluent: Petroleum ether/Ethyl acetate=5:1) to yield the desired compound.

3-F-6-CF_3-AD-Py: pale yellow solid (1.70 g), yield: 64.20%. ^{1}H NMR (500 MHz, $CDCl_3$) δ 8.73 (s, 1H), 8.65 (d, *J* = 8.4 Hz, 1H), 8.61-8.52 (m, 1H), 7.95 (d, *J* = 8.0 Hz, 1H), 7.50 (d, *J* = 8.4 Hz, 1H), 7.39 (d, *J* = 7.7 Hz, 1H), 7.03 (t, *J* = 8.4 Hz, 1H), 6.87 (s, 1H), 6.28 (d, *J* = 10.9 Hz, 1H), 2.60 (s, 3H).

1.3.2 General procedure for syntheses of PXZ-PAO and DPCz-PAO

In a dry 100 mL three-necked flask, 3-F-6-CF_3-AD-Py (600 mg, 1.67 mmol) was combined with phenoxazine (338 mg, 1.85 mmol) or diphenylamine-carbazole (927 mg, 1.85 mmol) and Cs_2CO_3 (1.09 g, 3.36 mmol). Anhydrous DMF was added to dissolve the contents, and the reaction mixture was refluxed at 165 °C under nitrogen for 12 h. Upon reaction completion, the solvent was evaporated under vacuum, and the resulting residue was partitioned with dichloromethane (DCM, 3×50 mL). The organic phases were pooled, dried with anhydrous sodium sulfate, and evaporated to dryness via rotary

evaporation, yielding the crude material. This was further purified via silica gel column chromatography using DCM as the eluent to obtain the target product. The crude product was further purified by repeated recrystallization from $CHCl_3$/CH_3OH to afford the pure compound.

PXZ-PAO: pale yellow solid (750 mg), yield: 83.92%. ^{1}H NMR (500 MHz, $CDCl_3$) δ 8.81 (d, *J* = 8.4 Hz, 1H), 8.74 (d, *J* = 8.3 Hz, 1H), 8.69 (d, *J* = 2.4 Hz, 1H), 7.92 (dd, *J* = 7.8, 2.3 Hz, 1H), 7.56 (dd, *J* = 8.0, 1.3 Hz, 1H), 7.40 (d, *J* = 7.9 Hz, 1H), 7.35-7.30 (m, 1H), 6.93 (d, *J* = 1.7 Hz, 1H), 6.79-6.44 (m, 7H), 5.98 (d, *J* = 8.0 Hz, 2H), 2.58 (s, 3H). ^{13}C NMR (150 MHz, Chloroform-*d*) δ 175.88, 151.54, 147.47, 143.66, 143.06, 141.18, 140.23, 134.87, 134.21, 134.00, 133.78, 133.57 129.97, 127.82, 123.27, 122.97, 122.71, 122.31, 121.46, 121.11, 120.47, 117.33, 117.31, 117.29, 117.27 114.50, 112.75, 112.72, 112.69, 112.66, 112.48, 17.37. MALDI-TOF-MS (*m/z*): calcd for $C_{32}H_{20}F_3N_3O_2$ 535.1502, found 535.1500 [M^+]. Anal. Calcd. for $C_{32}H_{20}F_3N_3O_2$: C, 71.77; H, 3.76; N, 7.85; Found: C, 71.71; H, 3.77; N, 7.84.

DPCz-PAO: pale yellow solid (1.15 g), yield: 80.7%. ^{1}H NMR (500 MHz, $CDCl_3$) δ 8.80 (d, *J* = 8.5 Hz, 1H), 8.75 (d, *J* = 8.4 Hz, 1H), 8.71 (d, *J* = 2.4 Hz, 1H), 7.93 (dd, *J* = 8.0, 2.4 Hz, 1H), 7.73 (s, 2H), 7.64-7.59 (m, 1H), 7.57 (d, *J* = 9.0 Hz, 1H), 7.47 (d, *J* = 7.8 Hz, 1H), 7.37 (d, *J* = 8.8 Hz, 2H), 7.28-7.18 (m, 10H), 7.08 (dt, *J* = 8.5, 2.7 Hz, 8H), 6.98 (q, *J* = 5.6 Hz, 5H), 6.85 (s, 1H), 2.53 (s, 3H). ^{13}C NMR (125 MHz, Chloroform-*d*) δ176.74, 152.40, 148.79, 143.97, 142.21, 141.47, 141.09, 137.26, 135.82, 129.71, 129.11, 128.84, 125.81, 124.60, 124.07, 122.90, 121.92, 120.31, 118.31,

113.61, 113.34, 110.88, 18.34. MALDI-TOF-MS (*m/z*): calcd for $C_{56}H_{38}F_3N_5O$ 853.3023, found 853.3053 [M^+]. Anal. Calcd. for $C_{56}H_{38}F_3N_5O$: C, 78.77; H, 4.49; N, 8.20; Found: C, 78.74; H, 4.47; N, 8.18

2. Dynamics parameters calculation

The kinetic parameters of the excited state are derived based on the listed equations S1-S8.[1] The contributions of the prompt (Φ_{PF}) and the delayed (Φ_{DF}) components to the total PLQY (Φ_{PL}) are obtained from the DF curves, using a biexponential function.

$$k_r = \Phi_{PF} / \tau_{PF} \quad \text{(S1)}$$

$$\Phi_{PL} = k_r/(k_r + k_{IC}) \quad \text{(S2)}$$

$$\Phi_{PF} = k_r/(k_r + k_{IC} + k_{ISC}) \quad \text{(S3)}$$

$$\Phi_{IC} = k_{IC}/(k_r + k_{IC} + k_{ISC}) \quad \text{(S4)}$$

$$\Phi_{ISC} = \frac{k_{ISC}}{k_r + k_{IC} + k_{ISC}} = 1 - \Phi_{PF} - \Phi_{IC} \quad \text{(S5)}$$

$$\Phi_{RISC} = \Phi_{DF}/\Phi_{ISC} \quad \text{(S6)}$$

$$k_{RISC} = (k_p k_d \Phi_{DF})/(k_{ISC}\Phi_{PF}) \quad \text{(S7)}$$

$$k_p = 1/\tau_{PF}, k_d = 1/\tau_{DF} \quad \text{(S8)}$$

3. Supplementary tables and figures

Table S1 HOMO-LUMO Overlap Integral of PXZ-PAO and DPCz-PAO (Gaussian Calculation, a.u.)

Compound	Overlap Integral[a]	Overlap Integral[b][10^{-5}]
PXZ-PAO	0.1299	5.832
DPCz-PAO	0.2159	13.189

[a] Overlap Integral of norm of the two orbitals. [b] Overlap Integral of square of the two orbitals.

Table S2 The calculation results for PXZ-PAO and DPCz-PAO at the B3LYP/6-31G(d) level.

Compound	HOMO/LUMO [eV]	Eg [eV]	E_S [eV]	E_T [eV]	$\Delta E_{(S_1-T_1)}$ [eV]	f
PXZ-PAO	-4.76/-1.98	3.49	2.26	2.24	0.02	0.005
DPCz-PAO	-4.73/-1.90	2.83	2.50	2.39	0.11	0.126

Table S3 Calculated energy levels and orbital transition configurations for PXZ-PAO and DPCz-PAO at the B3LYP/6-31G(d) level.

PXZ-PAO	E_{cal} (eV)[a]	Dominant excitation
S_1	2.2583	H→L (97.1%)
T_1	2.2399	H→L (96.3%)
T_2	2.7035	H-1→L (95.2%)
T_3	2.8210	H→L+1 (86.7%), H→L+5 (7.7%)
T_4	2.8413	H→L+5 (57.7%), H→L+4 (15.5%), H→L+1 (11.8%)
DPCz-PAO	E_{cal} (eV)[a]	Dominant excitation
S_1	2.4953	H→L (99.0%)
T_1	2.3882	H→L (91.4%)
T_2	2.7215	H-1→L (88.0%)
T_3	2.7591	H-2→L (75.7%), H-3→L (11.7%)
T_4	2.7623	H→L+3 (83.2%)

[a] Excitation energy

Table S4 The calculation SOC matrix element values for PXZ-PAO and DPCz-PAO at the B3LYP/6-31G(d) level.

Compound	$\langle S_1\|\hat{H}_{SO}C\|T_1\rangle$ [cm^{-1}]	$\langle S_1\|\hat{H}_{SO}C\|T_2\rangle$ [cm^{-1}]	$\langle S_1\|\hat{H}_{SO}C\|T_3\rangle$ [cm^{-1}]
PXZ-PAO	0.09	0.95	1.90
DPCz-PAO	0.11	1.83	0.85

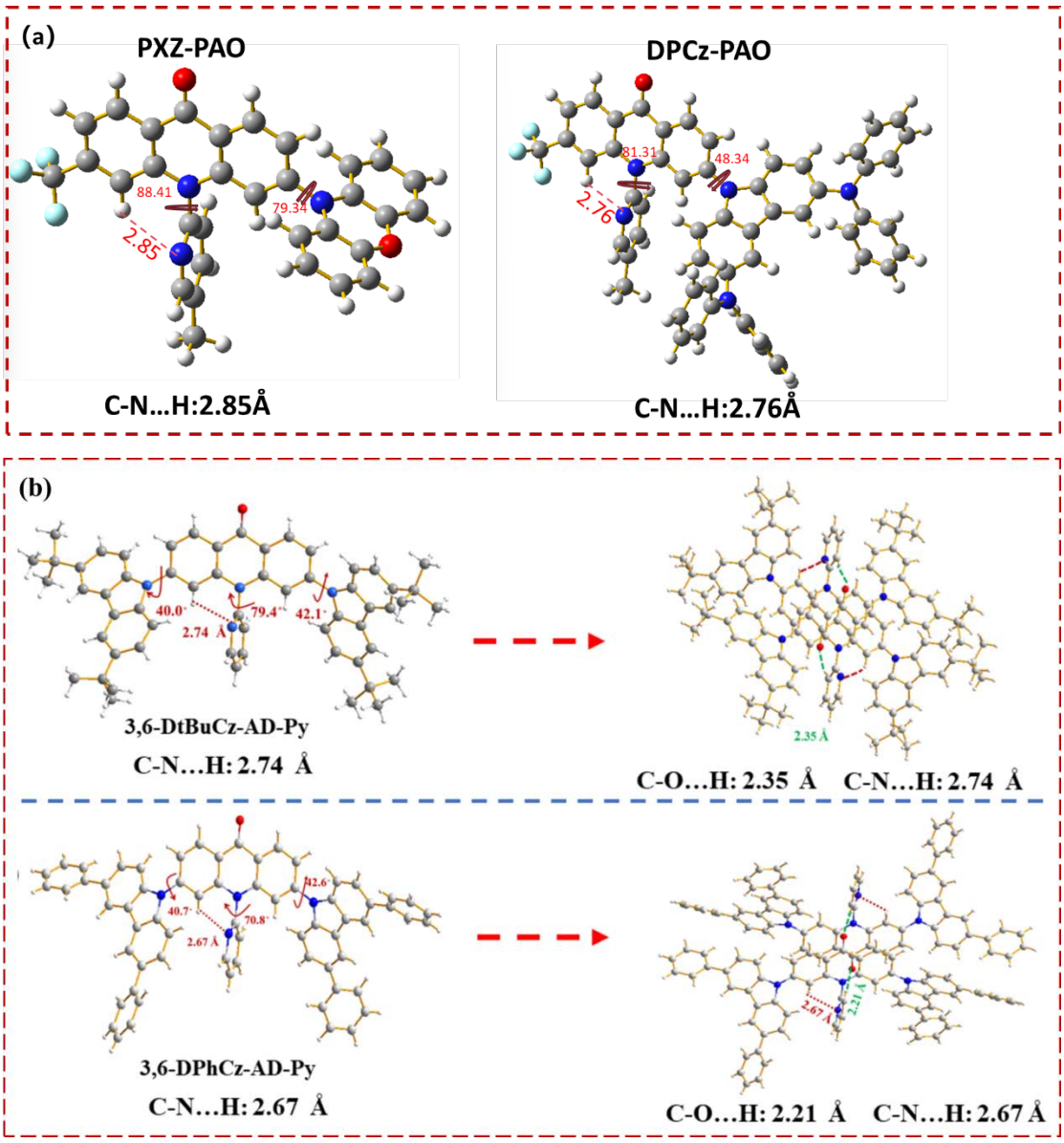

Fig. S1. (a) The optimized geometries of PXZ-PAO and DPCz-PAO determined by DFT calculation. (b) Single crystal geometries of the pyridyl-acridone derivatives with similar structures reported in literature.

(The calculated C-N...H distances in present PXZ-PAO and DPCz-PAO are almost identical to those observed in other pyridyl-acridone based analogues reported by our own group, confirming the presence of the intramolecular hydrogen bonds due to the incorporation of pyridyl ring at the 10-site of acridone acceptor.)

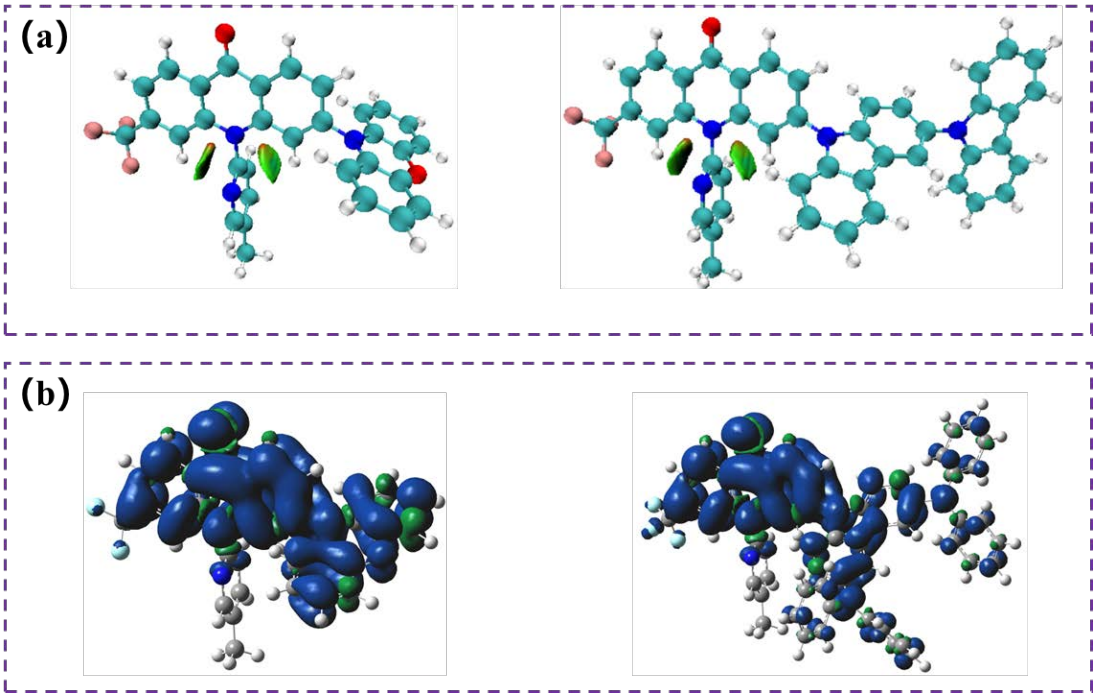

Fig. S2. The non-covalent interaction (NCI) isosurface maps (a) and triplet spin density distributions (TSDDs) (b) of PXZ-PAO and DPCz-PAO obtained by theoretical calculations.

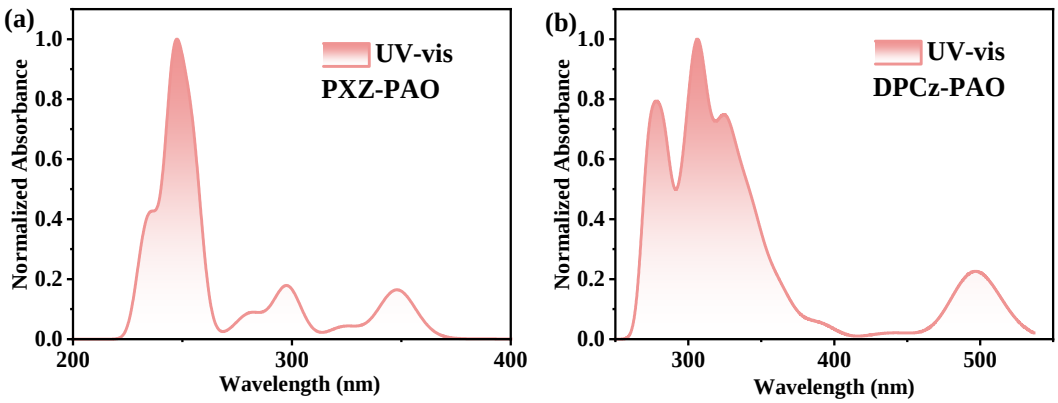

Fig. S3. The absorption spectra of PXZ-PAO and DPCz-PAO simulated by the TD-DFT method

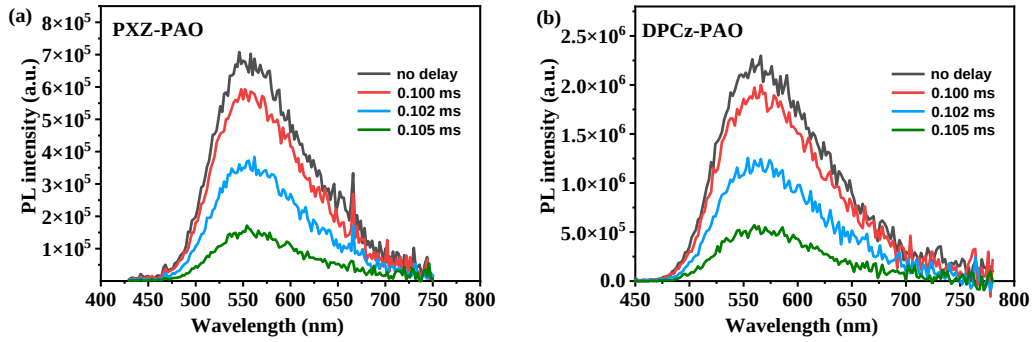

Fig. S4. Time-resolved spectra of (a) PXZ-PAO and (b)DPCz-PAO films in CBP host.

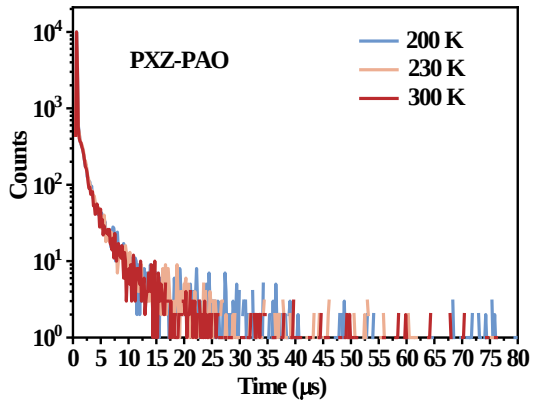

Fig. S5. Temperature-dependent transient PL decay curves of PXZ-PAO in doped films.

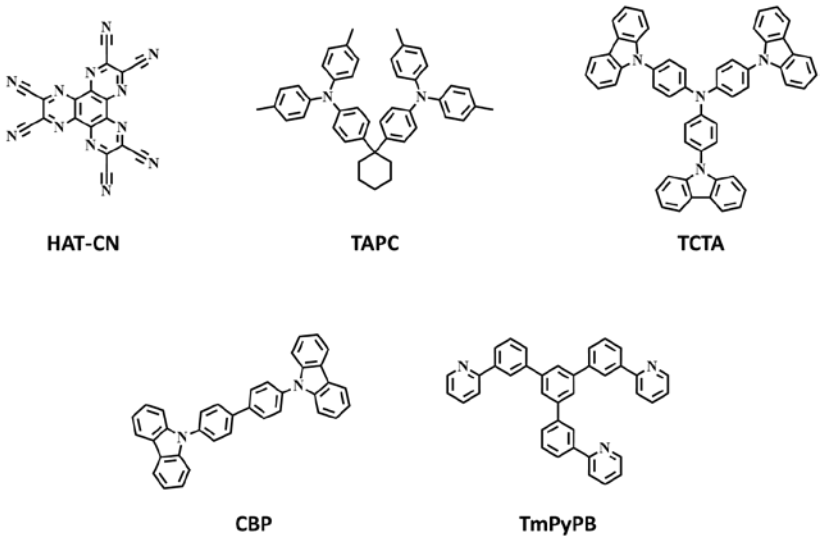

Fig. S6. Chemical structures of the materials utilized in present OLED fabrication.

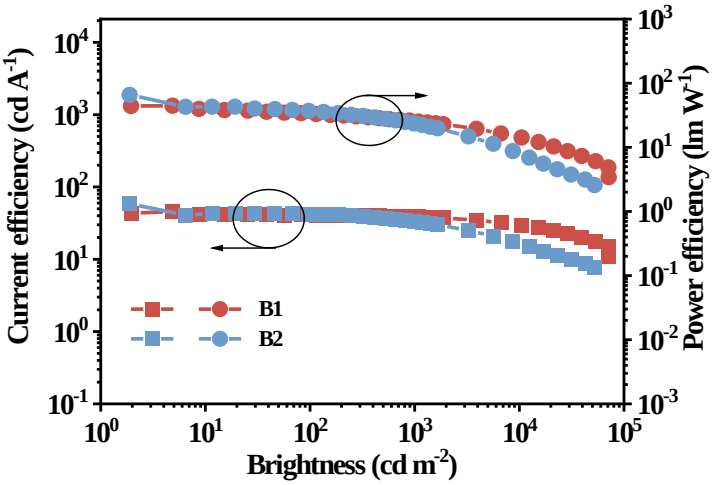

Fig. S7. CE and PE curves of PXZ-PAO (B1) and DPCz-PAO (B2) based OLEDs.

4. Mass spectroscopy and NMR spectra of the compounds

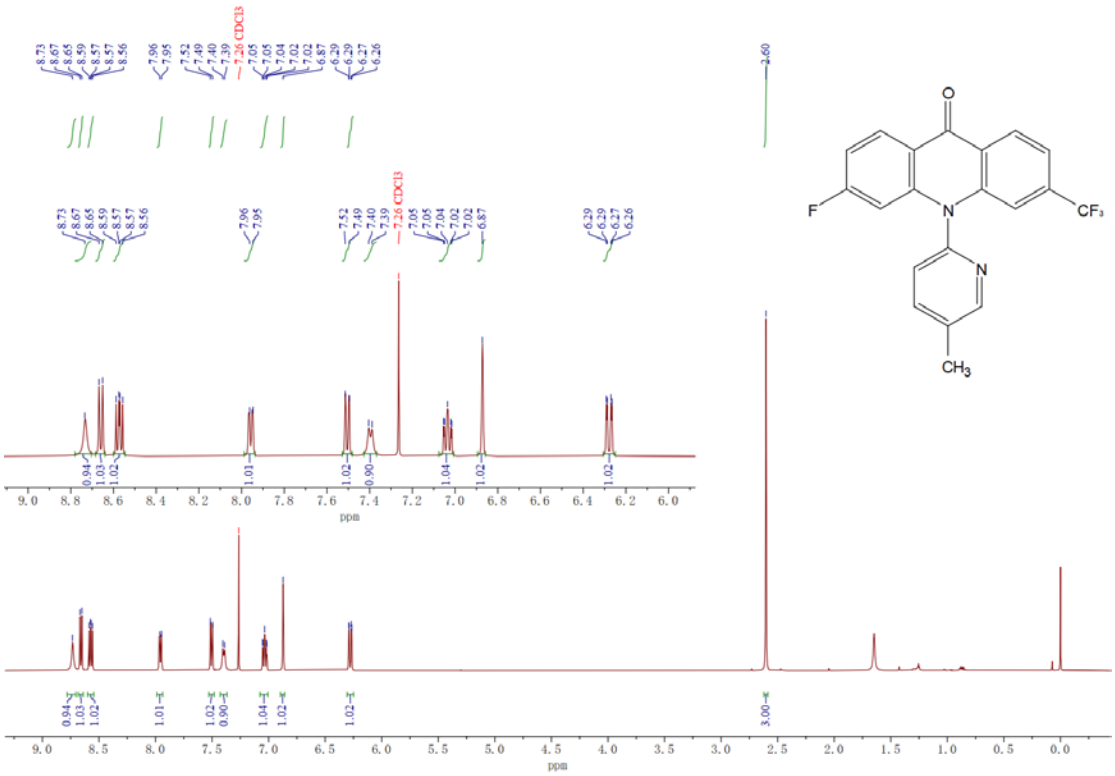

Fig. S8. ^{1}H NMR spectrum of 3-F-6-CF_3-AD-Py.

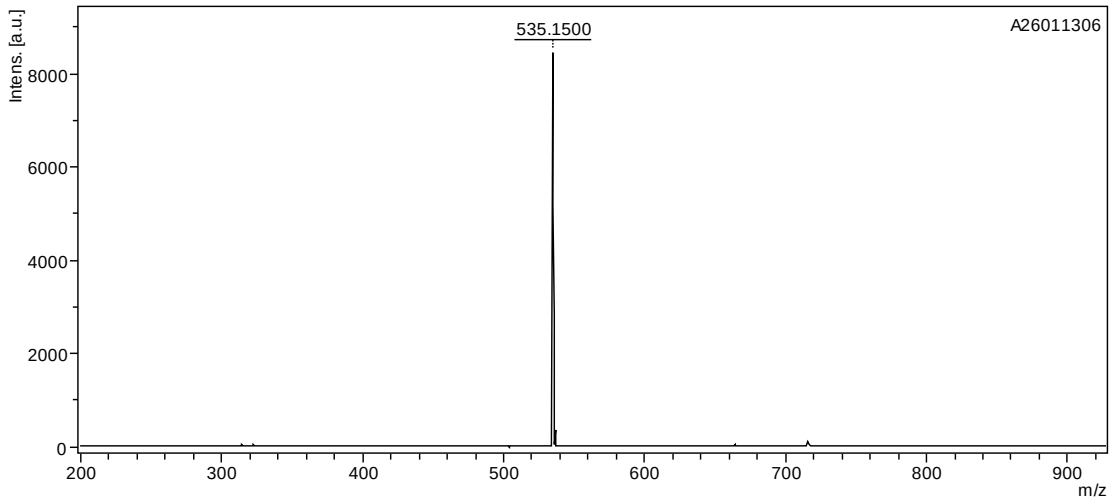

Fig. S9. HRMS of PXZ-PAO.

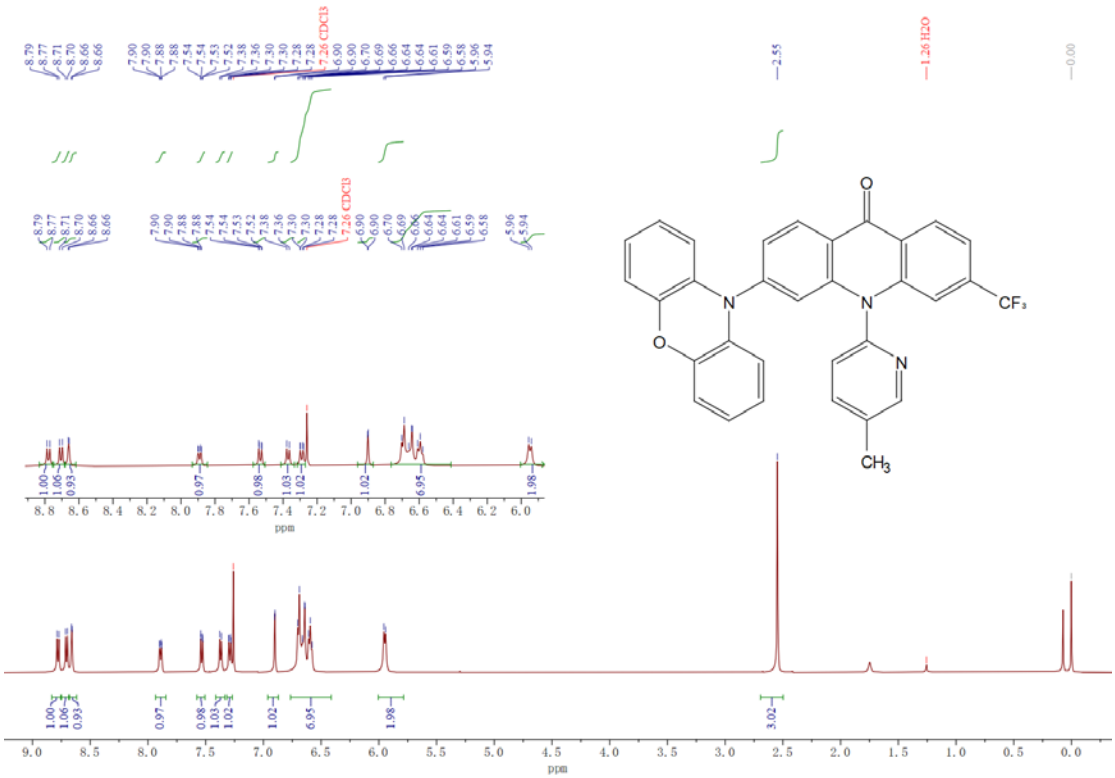

Fig. S10. ^{1}H NMR spectrum of PXZ-PAO.

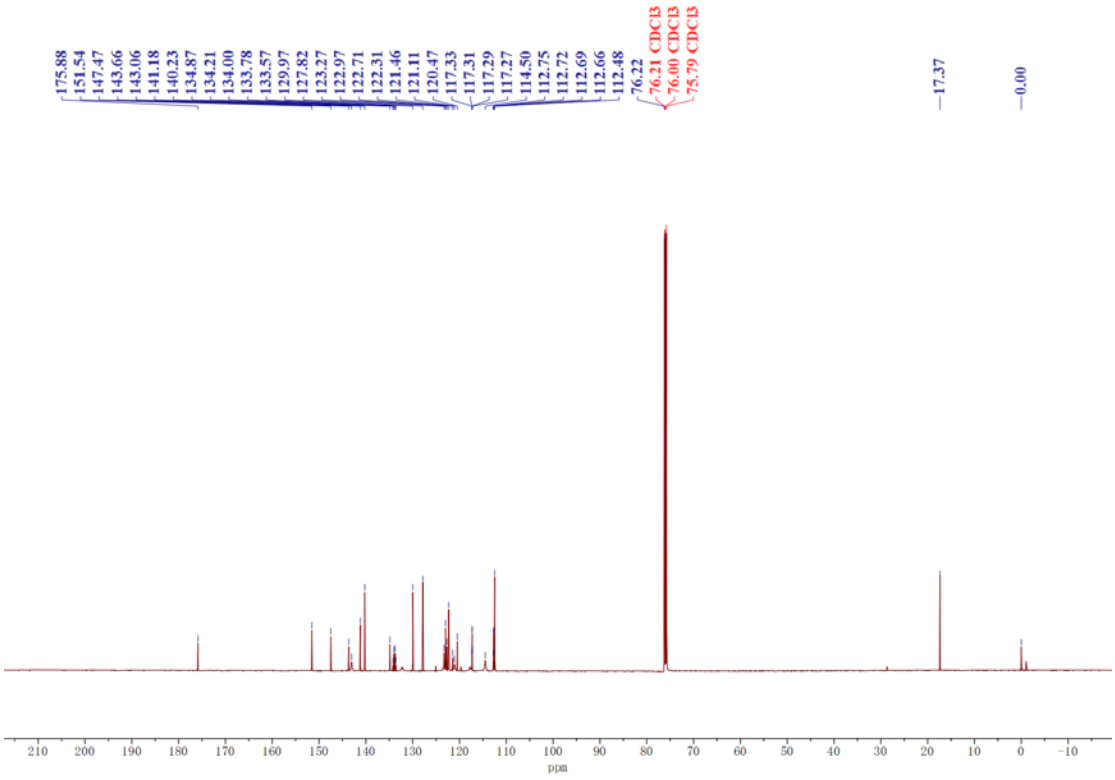

Fig. S11. ^{13}C NMR spectrum of PXZ-PAO.

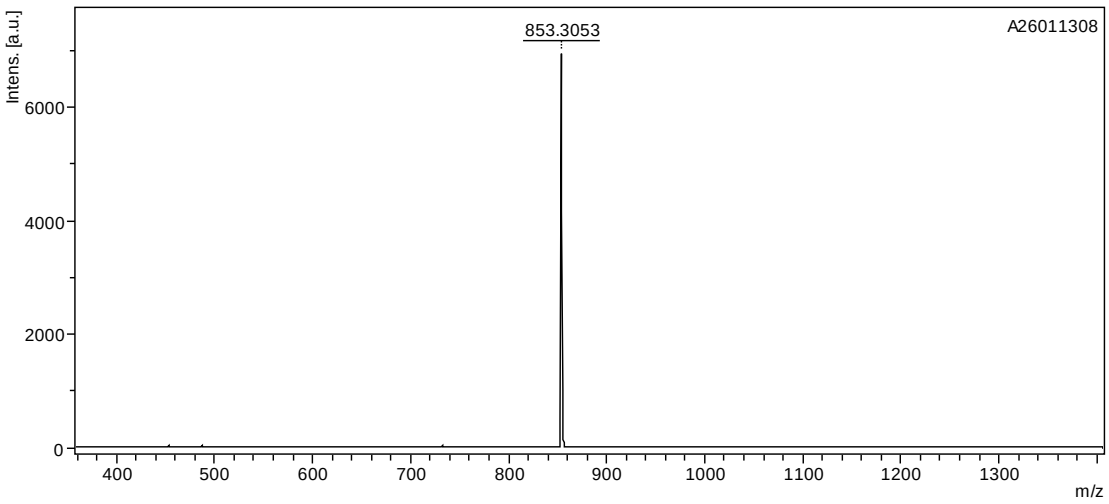

Fig. S12. HRMS of DPCz-PAO.

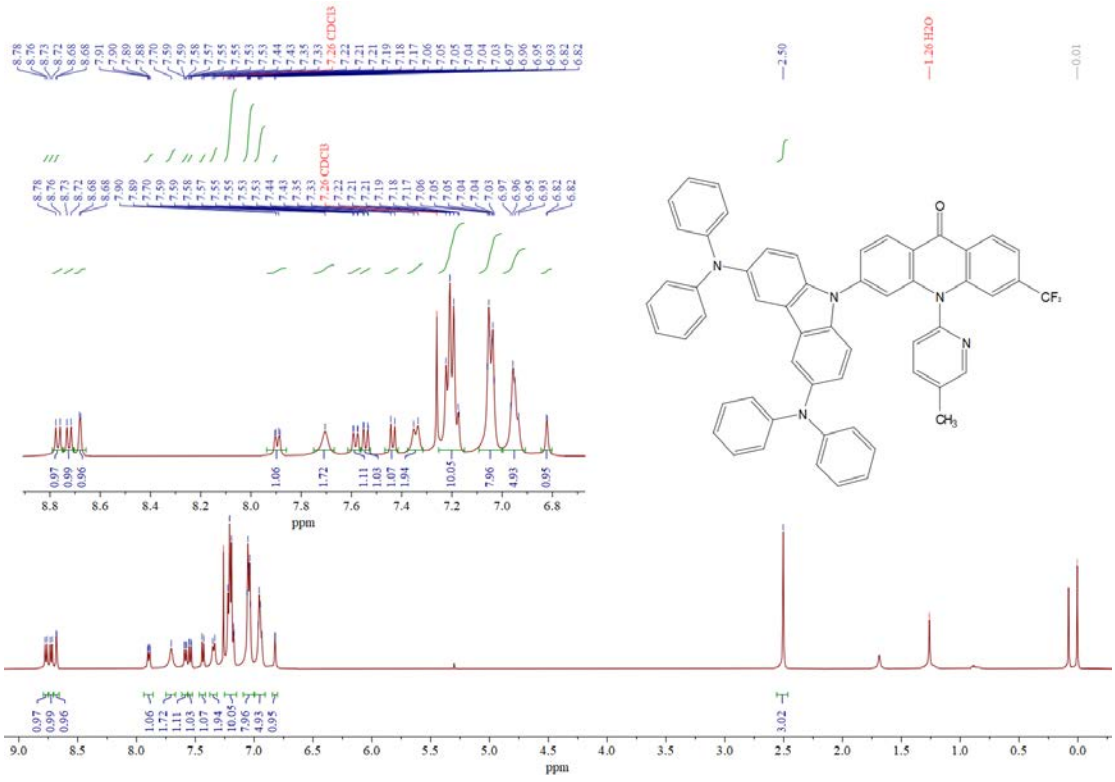

Fig. S13. ^{1}H NMR spectrum of DPCz-PAO.

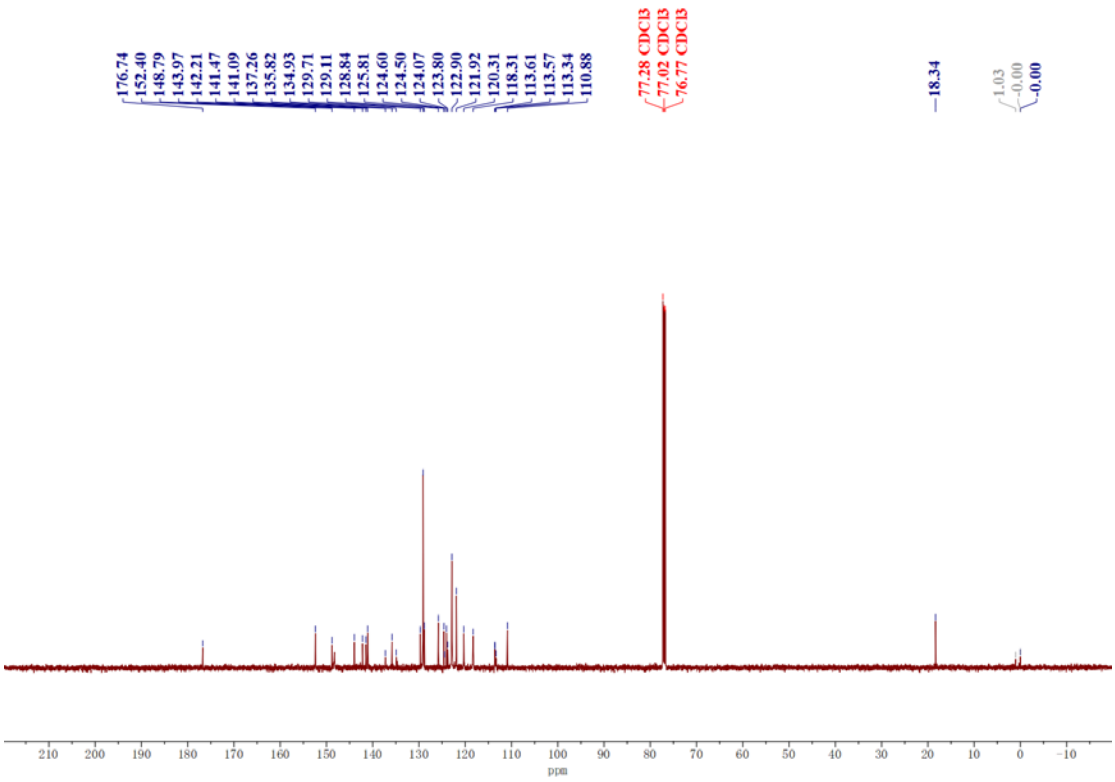

Fig. S14. ^{13}C NMR spectrum of DPCz-PAO.

4. References

[1] L. Gan, Z. Xu, Z. Wang, B. Li, W. Li, X. Cai, K. Liu, Q. Liang and S. J. Su, *Adv. Funct. Mater.*, 2019, **29**, 1808088.